Complexity of dynamical bifurcations in detuned degenerate four-wave mixing

Wang Kaige* and N. B. Abraham
Department of Physics, Bryn Mawr College, Bryn Mawr, Pennsylvania 19010-2899

L. A. Lugiato
Dipartimento di Fisica, Università degli Studi di Milano, via Celoria 16, 20133 Milano, Italy

M. Vadacchino
Dipartimento di Fisica del Politecnico, Corso Duca degli Abruzzi 24, 10129 Torino, Italy
(Received 28 September 1993)

We investigate numerically the dynamical bifurcations that occur in detuned degenerate four-wave mixing as the pump intensity is varied. We find several types of gluing bifurcations and symmetry-breaking bifurcations. A sequence of symmetric-breaking and gluing bifurcations leads to Lorenz-like chaos.

PACS number(s): 42.50.Ne, 05.45.+b, 42.65.Hw

I. INTRODUCTION

Interesting characteristics and dynamical behavior have been found in nonlinear optical systems involving two-photon processes. Such processes include second-harmonic generation, two-photon optical bistability, two-photon lasing, optical parametric oscillation, and four-wave mixing (FWM). These two-photon systems are of special interest because they show explicit macroscopic quantum characteristics, generating light with nonclassical statistical properties (e.g., squeezing) [1–6], which has been observed in recent experiments [7,8]. In the classical limit, these systems present rich and complicated instability behaviors [9–13]. It is useful for generalization to know that many of these two-photon systems have similar features [9,13,14]. In addition, the macroscopic quantum characteristics and the classical dynamical instabilities are related in some cases [6,15,16].

Four-wave mixing is a good example of many of these processes. It involves a two-photon process in both the pump field and the signal field. Earlier theoretical analyses and experimental observations of FWM have shown that squeezed light can be generated [2,17–19] and recently it was found that nearly perfect squeezing is possible for both the pump and signal modes in degenerate four-wave mixing (DFWM) [6]. For resonant DFWM, very complicated bifurcation behaviors have been found [13]. And, due to the dynamical asymmetry between the pump and signal modes, a Berry's phase analogy may occur in DFWM [20].

In this paper we analyze the instability conditions for both trivial and nontrivial solutions in the instability domain for detuned DFWM. Due to the dynamical symmetry of the equations with respect to inversion of the amplitude of the signal mode, the dynamics displays various symmetry breaking and gluing bifurcations. These processes are shown to lead to Lorenz chaos. However, our numerical results also show that a period doubling of intensities may occur in two ways: (a) normal period doubling of a periodic trajectory in the phase space and (b) apparent period doubling of a trajectory in the subspace of asymmetric variables combined with a symmetry breaking of the trajectory in the subspace of symmetric variables.

It is important to keep in mind that the model we use in this paper, which is taken from Ref. [2], holds only far from atomic resonances. More complete and complex models, which do not suffer from this limitation, can be found in [21–26].

II. THE SEMICLASSICAL EQUATIONS AND THE STATIONARY SOLUTIONS

We consider two fields, each close to resonance with a cavity mode (designated by subscripts 1 and 2), with annihilation operators of photons a_1 and a_2, frequencies ω_1 and ω_2, and losses γ_1 and γ_2, respectively. The two modes are coupled by a nonlinear medium which induces a DFWM process at frequency ω_0 close to ω_1 and ω_2. We assume modes 1 and 2 are different in some characteristic, such as wave vector or polarization [6]. Mode 1 is pumped by a coherent field at frequency ω_0.

Following Ref. [2], we assume that the dynamics of this system is governed by a master equation which can be written in the interaction picture as

$$\frac{d\rho}{dt} = -\frac{1}{\hbar}[H_F + H_E + H_I, \rho] + \sum_{j=1}^{2} \Lambda_j \rho \ , \tag{1}$$

where H_F is the free Hamiltonian of the two modes

$$H_F = \sum_{j=1}^{2} \hbar \Delta_j \gamma_j a_j^{\dagger} a_j \ , \tag{2}$$

with the detuning parameters Δ_j defined as

*Permanent address: Physics Department, Beijing Normal University, Beijing 100875, People's Republic of China.

$$\Delta_j=\frac{\omega_j-\omega_0}{\gamma_j} \quad (j=1,2) ; \tag{3}$$

H_E describes the action of the pump,

$$H_E=i\hbar E(a_1^\dagger-a_1) , \tag{4}$$

where the pump field amplitude E is taken real and positive for definiteness; H_I governs the FWM interaction

$$H_I=i\hbar\frac{\kappa}{2}(a_1^2a_2^{\dagger 2}-a_1^{\dagger 2}a_2^2) , \tag{5}$$

where κ is the coupling constant proportional to the nonlinear susceptibility $\chi^{(3)}$; and the Liouville operator Λ_j $(j=1,2)$ describes the losses of the modes in the cavity

$$\Lambda_j\rho=\gamma_j\{[a_j,\rho a_j^\dagger]+[a_j\rho,a_j^\dagger]\} . \tag{6}$$

In the deterministic semiclassical approximation, one neglects all fluctuations and their correlations. The resulting semiclassical equations are [2]

$$\dot{\alpha}_1=E-\gamma_1(1+i\Delta_1)\alpha_1-\kappa\alpha_1^*\alpha_2^2 , \tag{7a}$$

$$\dot{\alpha}_2=-\gamma_2(1+i\Delta_2)\alpha_2+\kappa\alpha_2^*\alpha_1^2 , \tag{7b}$$

where α_1 and α_2 indicate the mean values of a_1 and a_2, respectively. By introducing the normalized variables

$$A_1\equiv\left[\frac{\kappa}{\gamma_2}\right]^{1/2}\alpha_1 ,$$
$$A_2\equiv\left[\frac{\kappa}{\gamma_1}\right]^{1/2}\alpha_2 , \tag{8}$$
$$\bar{E}\equiv\frac{E}{\gamma_1}\left[\frac{\kappa}{\gamma_2}\right]^{1/2} ,$$

the semiclassical equations for DFWM become

$$\gamma_1^{-1}\dot{A}_1=\bar{E}-(1+i\Delta_1)A_1-A_1^*A_2^2 , \tag{9a}$$

$$\gamma_2^{-1}\dot{A}_2=-(1+i\Delta_2)A_2-A_1^2A_2^* . \tag{9b}$$

A_j $(j=1,2)$ denotes the normalized amplitude of mode j, and the A_j^*'s $(j=1,2)$ obey the complex conjugates of Eqs. (9a) and (9b). Exactly as in the case of the degenerate optical parametric oscillator [11], Eqs. (9) are symmetrical with respect to a change of sign in the signal field: if $\{A_1(t),A_2(t)\}$ is a solution of Eqs. (9), then $\{A_1(t),-A_2(t)\}$ is also a solution. For example, if the solutions are limit cycles, there are only two possible situations: (i) the trajectories of $\{A_1(t),A_2(t)\}$ and $\{A_1(t),-A_2(t)\}$ are identical, in which case the trajectory itself is symmetric with respect to the inversion of A_2, or (ii) the trajectories are not identical in the complex plane, in which case there are two solutions which are termed antisymmetric. For convenience we will refer to a variable for which the equations have this inversion symmetry (signal field) as a symmetric variable. The other variable (pump field) will be referred to asymmetric. In a four-dimensional phase space, these symmetries can be hard to visualize, but the trajectories upon inversion can be compared in the projection onto the complex plane for a symmetric variable. If the projection is symmetric upon inversion of both the real and imaginary parts of A_2, then the solution is symmetric [i.e., situation (i)].

The stationary solutions are obtained by setting $\dot{A}_1=\dot{A}_2=0$. There are two different kinds of stationary solutions.

(i) The trivial solution is

$$A_{2s}=0 , \tag{10a}$$

$$A_{1s}=\frac{\bar{E}}{1+i\Delta_1} . \tag{10b}$$

(ii) The nontrivial solutions, such that $|A_{2s}|^2\neq 0$, for which the intensities of the modes satisfy [6]

$$|A_{1s}|^2=\sqrt{1+\Delta_2^2} , \tag{11a}$$

$$|A_{2s}|^4+\frac{2(1-\Delta_1\Delta_2)}{\sqrt{1+\Delta_2^2}}|A_{2s}|^2+1+\Delta_1^2-\frac{|\bar{E}|^2}{\sqrt{1+\Delta_2^2}}=0 , \tag{11b}$$

and the complex amplitudes of the modes are

$$A_{1s}=\bar{E}\left[1+i\Delta_1+\frac{|A_{2s}|^2(1-i\Delta_2)}{\sqrt{1+\Delta_2^2}}\right]^{-1} , \tag{12a}$$

$$A_{2s}=\pm\left[\frac{\bar{E}-(1+i\Delta_1)A_{1s}}{A_{1s}^*}\right]^{1/2} . \tag{12b}$$

As in the case of the optical parametric oscillators [11], the steady-state curve of $|A_{2s}|^2$ as a function of $|\bar{E}|^2$ is multivalued when

$$\Delta_1\Delta_2>1 . \tag{13}$$

Under this condition there is a possibility of bistability between the trivial solution and the positively sloped part of the nontrivial stationary solutions (see Ref. [11]). For convenience and uniqueness, we will use the value of $|A_{2s}|^2$ to identify a particular steady-state solution in the phase space (as is common in studies of bistable optical systems).

III. LINEAR STABILITY ANALYSIS

By the linearization of Eqs. (9) with respect to the fluctuations δA_1 and δA_2, we obtain

$$\delta\dot{A}_1=-\gamma_1[(1+i\Delta_1)\delta A_1+A_{2s}^2\delta A_1^*+2A_{2s}A_{1s}^*\delta A_2] , \tag{14a}$$

$$\delta\dot{A}_2=-\gamma_2[-2A_{1s}A_{2s}^{*}\delta A_1+(1+i\Delta_2)\delta A_2-A_{1s}^{2}\delta A_2^{*}]\ , \tag{14b}$$

where we have indicated the stationary values of these variables by A_{1s} and A_{2s}.

Solutions of the form

$$\begin{pmatrix}\delta A_1\\ \delta A_1^{*}\\ \delta A_2\\ \delta A_2^{*}\end{pmatrix}=\exp(\lambda t)\begin{pmatrix}b_1\\ b_2\\ b_3\\ b_4\end{pmatrix} \tag{15}$$

give the eigenvalue equation

$$\begin{vmatrix}(1+i\Delta_1)+\lambda/\gamma_1 & A_{2s}^{2} & 2A_{2s}A_{1s}^{*} & 0\\ (A_{2s}^{*})^2 & (1-i\Delta_1)+\lambda/\gamma_1 & 0 & 2A_{2s}^{*}A_{1s}\\ -2A_{1s}A_{2s}^{*} & 0 & (1+i\Delta_2)+\lambda/\gamma_2 & -A_{1s}^{2}\\ 0 & -2A_{1s}^{*}A_{2s} & -(A_{1s}^{*})^2 & (1-i\Delta_2)+\lambda/\gamma_2\end{vmatrix}=0\ . \tag{16}$$

For the trivial solution, it is easy to obtain the instability condition

$$|A_{1s}|^2>\sqrt{1+\Delta_2^2} \tag{17a}$$

or, equivalently,

$$|\bar{E}|^2>(1+\Delta_1^2)\sqrt{1+\Delta_2^2}\ . \tag{17b}$$

For the nontrivial solution, the eigenvalue equation is

$$\lambda^4+c_1\lambda^3+c_2\lambda^2+c_3\lambda+c_4=0\ , \tag{18}$$

where

$$c_1=2\gamma_2(1+\mu)\ , \tag{19a}$$

$$c_2=\gamma_1\gamma_2[4+\mu(1+\Delta_1^2)+8\sqrt{1+\Delta_2^2}|A_{2s}|^2-\mu|A_{2s}|^4]\ , \tag{19b}$$

$$c_3=2\gamma_1^2\gamma_2\left[(1+\Delta_1^2)+4\sqrt{1+\Delta_2^2}\left[1+\frac{1}{\mu}\right]|A_{2s}|^2-|A_{2s}|^4\right]\ , \tag{19c}$$

$$c_4=4\gamma_1^2\gamma_2^2[2\sqrt{1+\Delta_2^2}(1-\Delta_1\Delta_2)|A_{2s}|^2+2(1+\Delta_2^2)|A_{2s}|^4]\ , \tag{19d}$$

and

$$\mu\equiv\frac{\gamma_1}{\gamma_2}\ . \tag{19e}$$

By the Routh-Hurwitz criterion, the necessary and sufficient conditions that the solution is stable are

$$c_1\geq 0 \tag{20a}$$

$$c_4\geq 0\ , \tag{20b}$$

$$c_1c_2-c_3\geq 0\ , \tag{20c}$$

$$(c_1c_2-c_3)c_3-c_1^2c_4\geq 0\ . \tag{20d}$$

To see which of these conditions controls the onset of instabilities, we examine each in turn. Condition (20a) is always satisfied. To evaluate condition (20b), one can reformulate c_4 as

$$c_4=4\gamma_1^2\gamma_2^2\sqrt{1+\Delta_2^2}|A_{2s}|^2\frac{d|\bar{E}|^2}{d|A_{2s}|^2}\ , \tag{21}$$

where the derivative is calculated from Eq. (11b). As expected, c_4 becomes negative on the negatively sloped part of the steady-state curve of $|A_{2s}|^2$ vs $|\bar{E}|^2$, indicating that this region is unstable [11]. The critical points of condition (20c) (i.e., $c_1c_2-c_3=0$) are located in the unstable region determined by condition (20d) if c_4 is positive (which is true for the positively sloped part of the steady-state curve) [cf. Eq. (21)]. Condition (20d) is violated when there are Hopf bifurcations on the positively sloped parts of the steady-state curves. Therefore, the critical points for loss of stability on the positively sloped branch are governed by equality in condition (20d). The frequency of the Hopf bifurcation at the bifurcation threshold is

$$\Omega_{\rm th}=\left[\frac{c_3}{c_1}\right]^{1/2}=\gamma_1\left\{\frac{1}{1+\mu}\left[(1+\Delta_1^2)+4\sqrt{1+\Delta_2^2}\left[1+\frac{1}{\mu}\right]|A_{2s}|^2-|A_{2s}|^4\right]\right\}^{1/2}\ . \tag{22}$$

In contrast to the case of the optical parametric oscillator [11], where bistability and spontaneous oscillation are mutually exclusive, spontaneous oscillations exist for both single-valued and multivalued steady-state curves.

Figure 1 shows the instability domains in the plane of the variables $|A_{2s}|^2$ and Δ_1, where we have set $\mu=1$, and we have drawn curves for five different values of $\Delta_2=-3$, 0, 1, 3, and 5. As indicated by our examples of $\Delta_2=3.0$

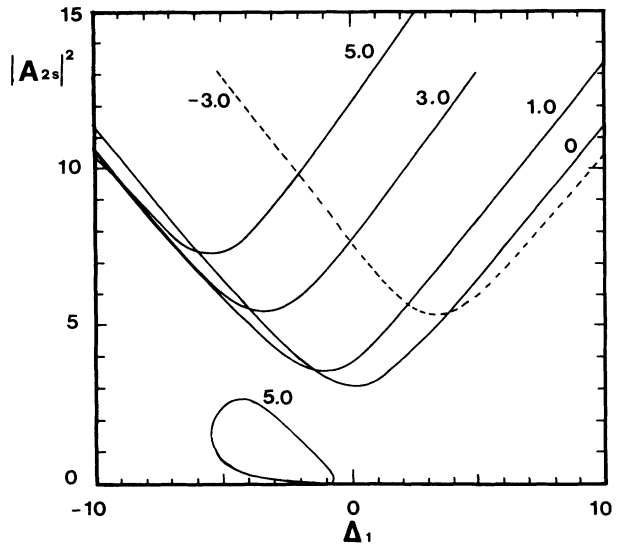

FIG. 1. Instability boundaries for the DFWM model in the plane of the detuning Δ_1 and the steady-state intensity of the signal mode $|A_{2s}|^2$ for $\mu=1.0$ and $\Delta_2=0$, 1, 3, 5, and -3, as labeled. The instability domains are above the parabolic curves, as well inside the lower circle.

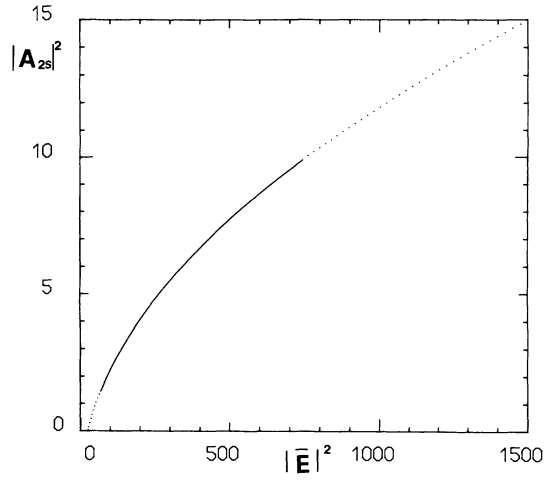

FIG. 2. Steady-state curve of the input intensity $|\bar{E}|^2$ versus the intensity of the signal mode $|A_{2s}|^2$ for $\mu=1.0$, $\Delta_1=-2.0$, and $\Delta_2=5.0$. The dotted parts of the curve are unstable.

and -3.0, according to Eqs. (19), when Δ_2 changes its sign, the corresponding boundary curves of the instability domain are mirror images with respect to the vertical axis at $\Delta_1=0$. Instabilities occur for values of $|A_{2s}|^2$ above the V-shaped boundaries. For large detuning of the signal field Δ_2, there is also an isolated instability domain very near the oscillation threshold of the signal field. We have studied the instabilities in this region more thoroughly, because they may be observed more easily in experiments.

IV. NUMERICAL SOLUTIONS

We have solved Eqs. (9) numerically for $\mu=1$, $\Delta_1=-2$, $\Delta_2=5$, and increasing steady-state values of $|A_{2s}|^2$ (equivalent to increasing the input field $\bar{E}$) under conditions where the steady-state curve is single valued. The steady-state curve for these parameters is shown in Fig. 2, where the dotted parts of the curve are unstable, and a very small stable region ($0<|A_{2s}|^2<0.0065$) is not visible. There are two unstable portions, one bounded and one unbounded. The existence of these two unstable domains can be ascribed to the fact that the interaction Hamiltonian for DFWM is of the two-photon type both for the pump and for the signal mode, and therefore this system is simultaneously similar to the case of degenerate parametric oscillations and to the case of second-harmonic generation. The unbounded unstable domain, which also exists in the resonant case, is similar to the instability typical of second-harmonic generation [9,10], while the bounded unstable domain, which exists only in detuned configurations, seems related to the oscillatory instability in detuned degenerate optical parametric oscillators [11].

The bounded instability domain leads to two branches of time-dependent solutions. For convenience we give the names of "lower" and "upper" to these two branches, according to the ranges of values of $|A_{2s}|^2$ in which they appear. The lower branch lies in the domain

$$0.0065<|A_{2s}|^2<0.124\ ,$$

and the upper branch is found in the domain

$$0.117<|A_{2s}|^2<1.47\ .$$

Either solution may be found in the range

$$0.117<|A_{2s}|^2<0.124\ .$$

Figure 3 shows some projections of the trajectory in the

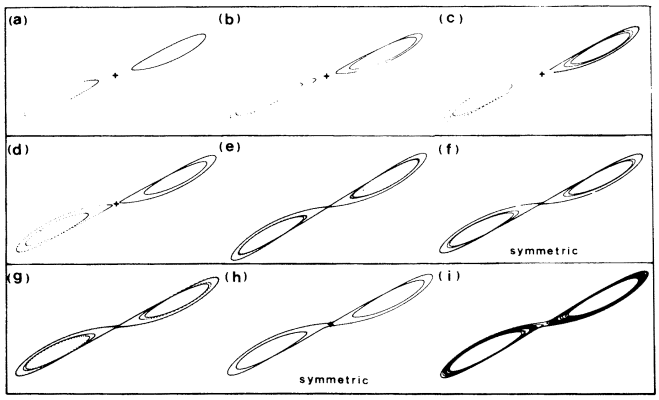

FIG. 3. Orbits in the complex plane of the signal mode for solutions on the lower branch in the isolated unstable domain for $\mu=1.0$, $\Delta_1=-2.0$, and $\Delta_2=5.0$, and for different steady-state intensities of the signal field $|A_{2s}|^2$: (a) 0.1, (b) 0.105, (c) 0.11, (d) 0.113 51, (e) 0.113 52, (f) 0.115 106, (f) 0.115 107, (h) 0.117, and (i) 0.12. Dotted orbits are the coexisting solutions obtained by inversion of A_2. The origin is indicated by a "+."

complex plane of the signal mode amplitude for the "lower" branch of solutions for different values of $|A_{2s}|^2$. Projections of the trajectories onto the complex planes of both the pump and signal modes for solutions on the upper branch are shown in Fig. 4. For example, at $|A_{2s}|^2=0.1$ on the lower branch of solutions [see Fig. 3(a)], the orbits of the signal mode can be either one of a pair of simple asymmetric cycles (which one is reached depends on the initial condition), while at $|A_{2s}|^2=0.29$ on the upper branch of solutions the orbit of the signal mode becomes a large single cycle, which is symmetric with respect to the origin [see Fig. 4(a)]. The intermediate development of the attractors is not simply a "gluing" of two asymmetric solutions to form the symmetric one. Instead, in Fig. 3, we show that there is a period-doubling sequence which reaches at least period 4 and then returns to period 2 before being interrupted by a unusual gluing bifurcation [27–29]. The glued orbit [see Fig. 3(e)] is not a simple symmetric union of a pair of asymmetric orbits [Fig. 3(d)]; instead, it is still asymmetric: its partner solution [the dotted line in Fig. 3(c)] does not coincide with itself. As we increase the input field further, this asymmetric glued solution undergoes a period doubling and, then, gradually becomes symmetric, as shown in Fig. 3(f). At $|A_{2s}|^2=0.115\,107$, we see that there has been an ungluing; the trajectory has become one of a pair of asymmetric solutions [see Fig. 3(g)], which are similar to those found in Fig. 3(e). Then, these orbits gradually become symmetric again in Fig. 3(h). Near the end of this branch, chaos appears [Fig. 3(i)]. For values of the input field larger than 0.124, there is a jump to the upper branch—a periodic simple cycle with a symmetric configuration [similar to that shown in Fig. 4(a)].

The evolution of trajectories for the "upper" branch is more regular when $|A_{2s}|^2$ is increased. A basic stage of this evolution is shown in Fig. 4. While the orbit of the pump mode in the complex plane doubles its period, the symmetric orbit of the signal mode loses its symmetry gradually [see Figs. 4(a)–4(c)]. Then, a chaotic solution appears in which the chaotic attractor for the signal mode keeps the basic shape of the previous periodic one [Fig. 4(d)]. When $|A_{2s}|^2$ is increased further, a gluing of two chaotic attractors occurs in the chaotic motion [Fig. 4(e)]. [Note that because of the symmetry of the signal variable, there is an another chaotic solution for which the signal mode trajectory is the inverse of that shown in Fig. 4(d).] This new symmetric chaotic attractor for the signal mode evolves to a stable periodic cycle [Fig. 4(f)], with a period which is approximately twice that of the previous periodic solution [Fig. 4(c)]. This process repeats until a Lorenz-like chaos is formed (Fig. 5).

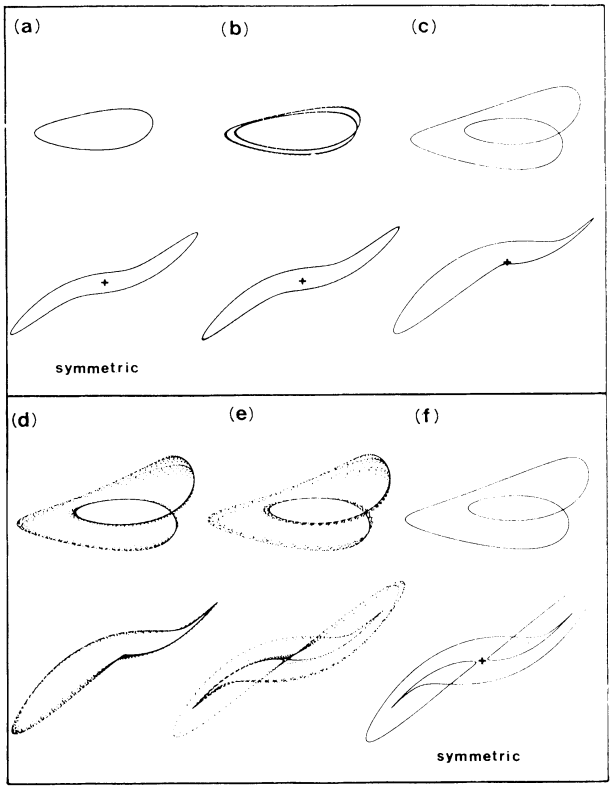

FIG. 4. Orbits in the complex planes of both pump (upper plots) and signal (lower plots) fields on the upper branch in the isolated unstable domain for $\mu=1.0$, $\Delta_1=-2.0$, and $\Delta_2=5.0$, and for different steady-state intensities of the signal field $|A_{2s}|^2$: (a) 0.29, (b) 0.33, (c) 0.35, (d) 0.37, (e) 0.38, and (f) 0.39. The origin is indicated by a "+" sign.

These developments are summarized in Table I, where (a) and (b) refer to the lower and upper branches, respectively. The notations P and C denote periodic and chaotic solutions, respectively; LC identifies chaotic behavior reminiscent of Lorenz chaos [30]. The subscripts s and a indicate symmetric and asymmetric orbits, respectively, and the superscripts ($\pm$) emphasize that there is a pair of

TABLE I. Development of bifurcations in the isolated instability domain indicated in Fig. 2: (a) Lower branch and (b) upper branch.

					(a) Lower branch						
$\lvert A_{2s}\rvert^2$	0.1	0.105	0.11–0.112	0.113–0.113 51	0.113 52	0.113 53–0.114	0.115–0.115 106	0.115 107	0.117	0.118–0.124	
Pump	$P(1)$	$P(2)$	$P(4)$	$P(2)$	$P(4)$	$P(8)$	$P(4)$	$P(4)$	$P(2)$	C	
Signal	$P_a^{\pm}(1)$	$P_a^{\pm}(2)$	$P_a^{\pm}(4)$	$P_a^{\pm}(2)$	$P_a^{\pm}(2,2)$	$P_a^{\pm}(4,4)$	$P_s(4,4)$	$P_a^{\pm}(2,2)$	$P_s(2,2)$	C	
					(b) Upper branch						
$\lvert A_{2s}\rvert^2$	0.117–0.29	0.3–0.35	0.37–0.38	0.39	0.4	0.41	0.415	0.42	0.43	· · ·	0.6–1.47
Pump	$P(1)$	$P(2)$	C	$P(2)$	$P(4)$	C	$P(4)$	$P(8)$	C	· · ·	LC
Signal	$P_s(1,1)$	$P_a^{\pm}(1,1)$	C	$P_s(2,2)$	$P_a^{\pm}(2,2)$	C	$P_s(4,4)$	$P_a^{\pm}(4,4)$	C	· · ·	LC

solutions symmetric to each other with respect to the origin. (Note that this is redundant as a always has $\pm$.) The numbers in the brackets indicate the number of intensity peaks in a period. In order to distinguish the intensity pulses of different phase for the complex amplitudes, we use two numbers in a bracket (n,m), indicating m pulses are approximately π out of phase with respect to n pulses. When, instead, there is only one number n in the bracket, this indicates that all the n pulses in a period are approximately in phase.

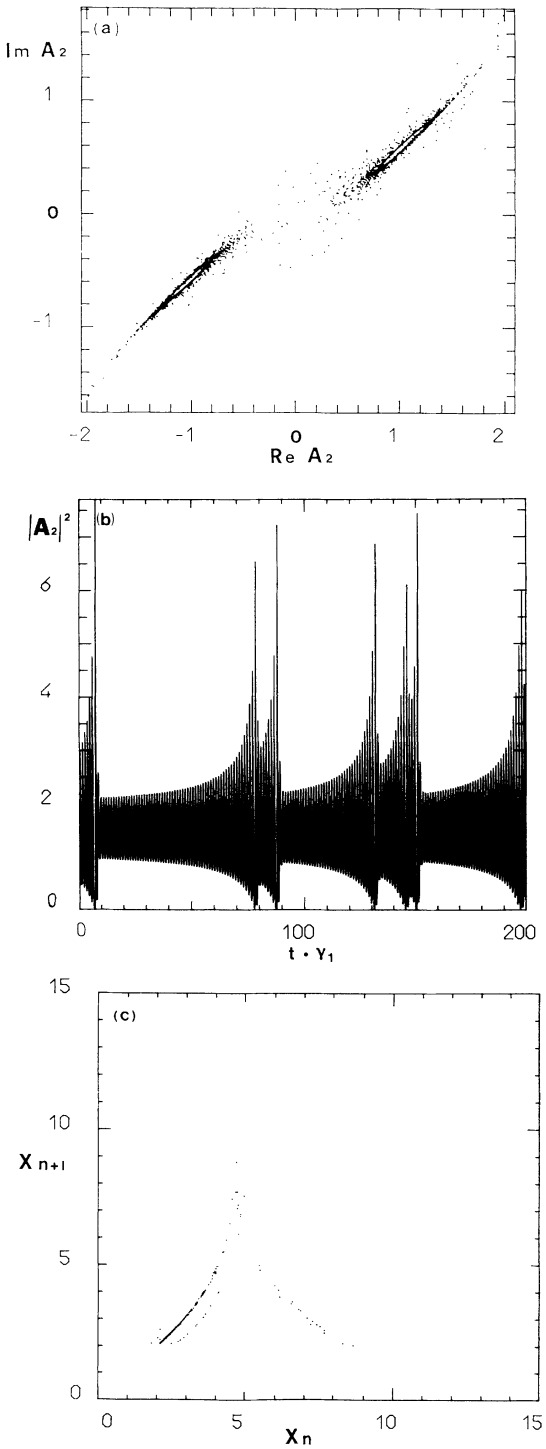

FIG. 5. Lorenz-like chaos for $\mu=1.0$, $\Delta_1=-2.0$, $\Delta_2=5.0$, and $|A_{2s}|^2=1.47$: (a) Orbit in the complex plane of the signal field, (b) intensity evolution in time for the signal field, and (c) Lorenz map for peaks in the intensity of the signal field.

We conclude by noting the following features for the time-dependent solutions in this bounded unstable domain in Fig. 2. (i) When the solution for the signal field is asymmetric, the signal and pump fields have the same period, while when the solution for the signal field is symmetric, its period is twice of that of the pump field. (ii) For the latter case in (i), the symmetric orbital (signal field) may not double its periodic directly [31]; instead, it breaks its symmetry which appears as a period doubling in the projection of the orbit onto the complex plane of the pump field. However, we see apparent period doubling of the intensity pulsations for both the pump and signal fields. (iii) For the upper branch, chaotic windows appear between transitions from asymmetric orbits to the gluing of these orbits into a symmetric orbit (or the inverse ungluing process). Through a sequence of symmetry breaking and gluing bifurcations that are mediated by chaos, i.e.,

$$\cdots \rightarrow P_s(n,n) \rightarrow P_a^{\pm}(n,n) \rightarrow C \rightarrow P_s(2n,2n) \rightarrow \cdots ,$$

one gets to Lorenz-like chaos [30]. These transitions are very similar to those found in Ref. [32], and have been discussed by Coullet and Tresser as a generalized route to the Lorenz-like chaos in systems with at least one symmetric variable.

We show the Lorenz-like characteristics of the chaotic solution in Fig. 5, where Fig. 5(a) shows the orbit of the signal mode, Fig. 5(b) is its intensity evolution, and Fig. 5(c) is a Lorenz map: in a long sequence of oscillations, we select the maximum intensities and arrange them in an ordered sequence X_i $(i=1,2,\ldots,n,n+1,\ldots)$, and then we plot X_{n+1} as a function of X_n.

In a small domain

$$1.457 < |A_{2s}|^2 < 1.470 ,$$

the stable steady-state solution and the Lorenz-like chaotic solution coexist. This indicates that the Hopf bi-

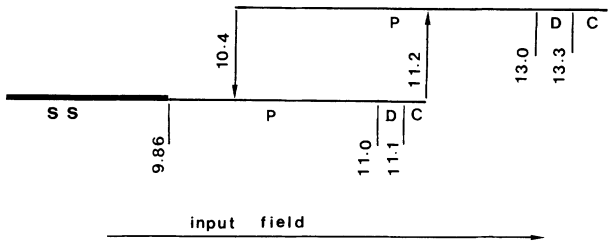

FIG. 6. Global behavior of the upper unstable domain versus the intensity of the signal field for $\mu=1.0$, $\Delta_1=-2.0$, and $\Delta_2=5.0$; the symbols SS, P, D, and C denote steady-state, periodic, period-doubled, and chaotic solutions, respectively. The labeled values are steady-state intensities of the signal field $|A_{2s}|^2$.

furcation of the steady state leading to the chaotic behavior is subcritical.

For the unbounded instability domain in Fig. 2 ($|A_{2s}|^2 > 9.859$), there are also two branches, whose global behavior is shown in Fig. 6. Simple periodic orbits appear in the lower branch and more complicated solutions are found on the upper branch, as shown in Fig. 7. We have not found gluing bifurcations in this unstable domain.

V. DISCUSSION

For some nonlinear dynamical systems, a subset of variables may possess a dynamical symmetry. That is, they may have some variables which can be inverted to obtain alternative solutions. We call these variables "symmetric variables." A typical example in nonlinear optical systems is the Lorenz-Haken model [30], where the real field and polarization are what we call symmetric variables. Another example in two-photon processes is the optical parametric oscillator, where the signal mode is symmetric. Some special bifurcation behaviors are involved in these systems, such as gluing bifurcations, symmetry breaking of symmetric orbits, and a route to Lorenz-like chaos. These phenomena are found here in the DFWM model, and we will discuss them phenomenologically.

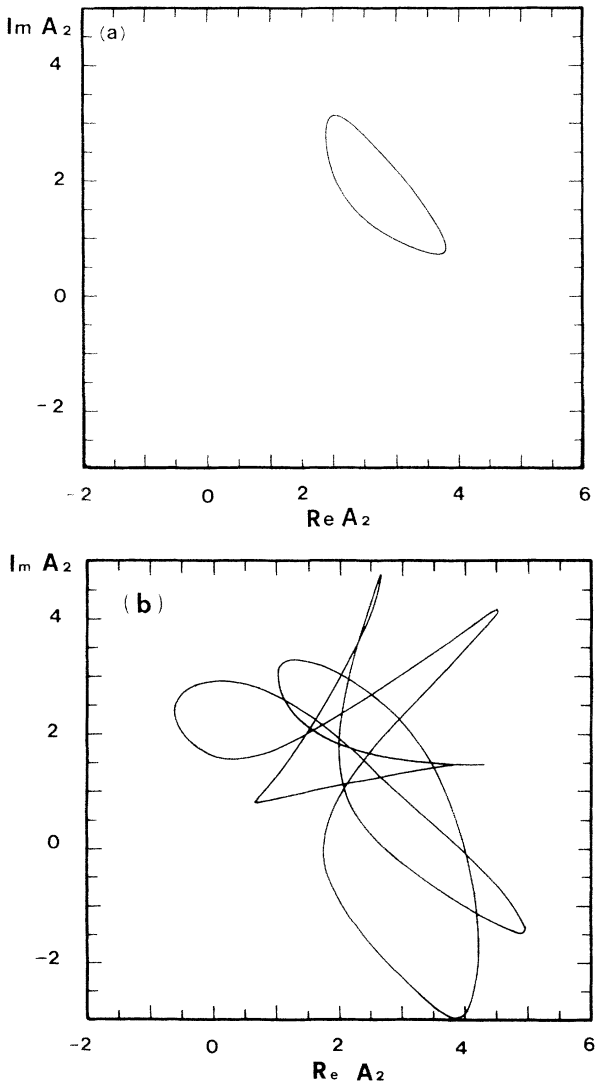

FIG. 7. Periodic orbits in the complex plane of the signal field in the upper unstable domain in Fig. 1 for $\mu=1.0$, $\Delta_1=-2.0$, $\Delta_2=5.0$, and $|A_{2s}|^2=10.5$: (a) periodic orbit on the lower branch of solutions and (b) periodic orbit on the upper branch of solutions.

For DFWM, as we have shown in the previous sections, there are two kinds of limit cycles: symmetric and asymmetric, assigned to the inversion symmetry of the orbits in the complex plane. Asymmetric orbits of the symmetric variable always appear in a pair, each of which corresponds to inversion of the other. Symmetric orbits satisfy time translation antisymmetry [31]:

$$A_2\left[t+\frac{T}{2}\right]=-A_2(t)\ , \tag{23}$$

where T is the period of the limit circle. That means, in the complex plane, the locus of the symmetric variable in the first half period is the inversion of the locus in second half-period. Hence its orbit is symmetric with respect to the origin in the complex plane. By a Fourier expansion of solutions satisfying Eq. (23), we can write for these symmetric orbits that

$$A_2(t)=\sum_{n=-\infty}^{\infty} a_{2n+1}\exp[2\pi i(2n+1)t/T]\ , \tag{24}$$

in which all the components with the even-harmonic frequencies, as well the constant term, vanish [33]. Note, however, that there are no other restrictions or symmetries placed on these a_j's.

The gluing bifurcation is one in which two limits cycles C_1 and C_2 come closer and closer to the point corresponding to the trivial stationary solution until they join, giving rise to a new stable periodic orbit which essentially follows successively the loci in phase space of the cycles C_1 and C_2 [28,29]. Its inverse process is termed an ungluing bifurcation. In most cases, C_1 and C_2 are a pair of orbits, symmetric to each other, so we can describe these bifurcations as $P_a^{\pm}(n) \Longleftrightarrow P_s(n,n)$ or $P_a^{\pm}(m,n) \Longleftrightarrow P_s(m+n,n+m)$.

For DFWM we have observed four types of symmetry changing bifurcations:

Type 1, supercritical gluing: $P_a^{\pm}(n,n) \Longleftrightarrow P_s(2n,2n)$. Two orbits, $P_a^{\pm}(n,n)$, become infinitesimally closer to each other at the point which corresponds to the trivial stationary solution and glue to form a symmetric orbit $P_s(2n,2n)$. An example is shown in Figs. 3(g) to 3(f). We notice that unglued asymmetric limit cycles of the signal mode in Fig. 3(g) are almost exactly half of the glued symmetric limit cycle. Hence, there is almost no trace of the bifurcation in the evolution of the intensity of either the pump or signal field, as shown in Fig. 8 (the only trace which can be found is a slight change of period, re-

sulting because the glued orbit is closer than unglued ones to the trivial stationary solution, where it spends a longer time). Apparently, this type of gluing may satisfy a topological condition—each half of the symmetric orbit is almost a closed limit cycle.

Type 2, gluing via chaos: $P_a^{\pm}(n,n) \Longleftrightarrow C \Longleftrightarrow P_s(2n,2n)$. A pair of orbit $P_a^{\pm}(n,n)$ glue to form a symmetric orbit $P_s(2n,2n)$ via chaotic processes [32]. An example has been shown in Figs. 4(c)–4(f), where the gluing process happens in chaotic motion. In the intensity evolution, we can expect that chaotic oscillations appear in between two very similar periodic oscillations, when the control parameter is changed. Topologically, this type of gluing can not occur through type 1, because half of the symmetric orbit is not a closed cycle.

The power spectra of both pump and signal modes are shown in Fig. 9, where Figs. 9(b) and 9(c) correspond to Fig. 4(c) ($|A_2|^2=0.35$) and Fig. 4(f) ($|A_{2s}|^2=0.39$), respectively. The spectrum of the pump mode has no significant change, and in the spectrum of the signal

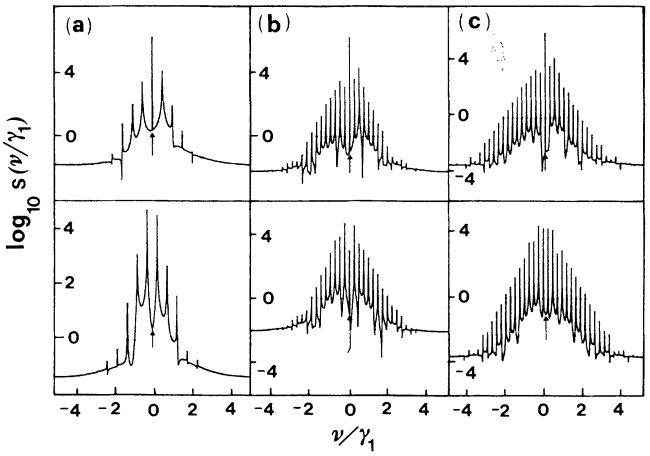

FIG. 9. Power spectra $s(\nu/\gamma_1)$ of the complex field amplitudes for both pump (upper plots) and signal fields (lower plots): (a) $|A_{2s}|^2=0.29$, (b) $|A_{2s}|^2=0.35$, and (c) $|A_{2s}|^2=0.39$, which correspond to Figs. 4(a), 4(c), and 4(f), respectively. The arrows indicate the reference frequency of the input field.

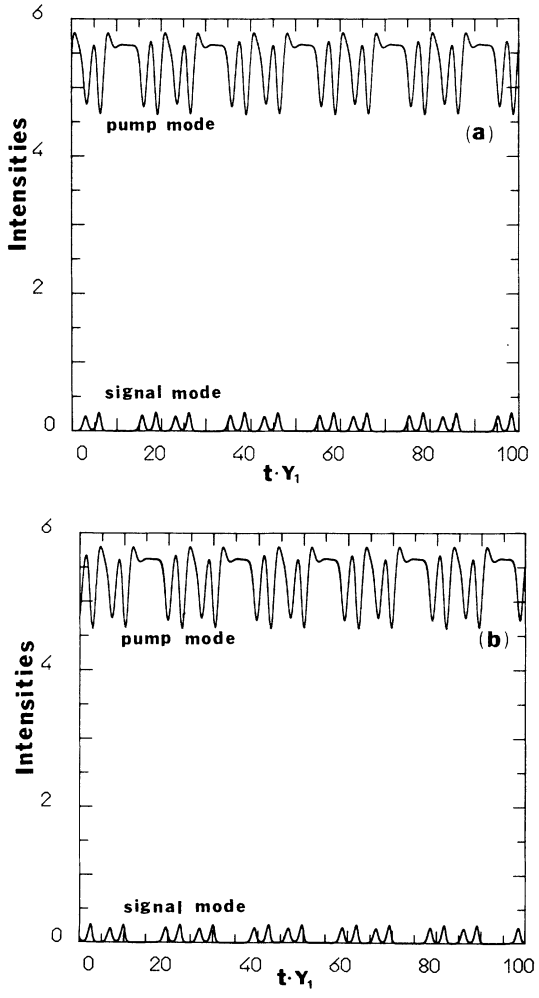

FIG. 8. Intensity evolution of both pump and signal fields for $\mu=1.0$, $\Delta_1=-2.0$, and $\Delta_2=5.0$ in the lower island of instability in Fig. 1: (a) $|A_{2s}|^2=0.115\,106$, symmetric orbit: (b) $|A_2|^2=0.115\,107$, asymmetric orbit. (a) and (b) correspond to Figs. 3(f) and 3(g), respectively.

mode a frequency shift of half of the frequency interval between the peaks can be observed. In fact, this is a result of combination of the two effects after gluing: the fundamental oscillation frequency is reduced by half and the even-harmonic frequency components vanish. The spectra of type-1 bifurcations are expected to be similar to those of type 2. Hence, this is a way to observe the evidence of the supercritical gluing bifurcation.

Type 3, abnormal gluing: $P_a^{\pm}(n) \Longleftrightarrow P_a^{+}(n,n)$ or $P_a^{-}(n,n)$. Two orbits come close to each other at the trivial stationary fixed point solution and glue into one of a pair of new joint orbits. We denote this as abnormal because the glued orbit is also asymmetric. A possible explanation is that the normal glued symmetric orbit is unstable. An example was shown in the transition from Fig. 3(d) to Fig. 3(e). In this case, both the pump and signal modes double their period, so in the intensity evolutions we observe a period-doubling bifurcation and their spectral changes are similar to those of a normal period-doubling bifurcation.

Type 4, gradual loss of symmetry: $P_s(n,n) \Longleftrightarrow P_a^{\pm}(n,n)$, Although the breaking of symmetry of orbits can occur in ungluing bifurcations of types 1 and 2, for definiteness, we note that there are also symmetry-breaking bifurcations [32,34] in which the symmetric orbit begins to gradually lose its symmetry. In this process the orbit of the asymmetric variable doubles its period. The inverse process is termed symmetry restoring. An example is shown in Figs. 4(a)–4(c). Intensity evolutions of both pump and signal modes appear as in a period-doubling oscillation. The before and after optical spectra are given in Fig. 9, where Figs. 9(a) and 9(b) correspond to Figs. 4(a) ($|A_{2s}|^2=0.29$) and 4(b) ($|A_{2s}|^2=0.35$), respectively. The changes of the spectra are very similar to those following a period-doubling bifurcation by means of the subharmonic generating process; the only difference is that before the symmetry breaking, the fundamental oscillation frequency of the pump field is twice that of the signal

field, but they still have same frequency spacing because all the even-harmonic components of the spectrum of the signal field disappear.

For the symmetric periodic solutions of the DFWM model, as many authors (see, e.g., [31]) have indicated should be the case, a symmetric orbit is never observed to bifurcate directly to a period-doubled limit cycle. However, a sequence of symmetry breaking and gluing bifurcations may be a route to reaching Lorenz-like chaos.

ACKNOWLEDGMENT

We are grateful to A. M. Albano for many useful suggestions and discussions.

[1] C. M. Savage and D. F. Walls, Phys. Rev. A **33**, 3282 (1986).
[2] C. M. Savage and D. F. Walls, J. Opt. Soc. Am. B **4**, 1514 (1987).
[3] A. S. Lane, M. D. Reid, and D. F. Walls, Phys. Rev. A **38**, 788 (1988).
[4] P. Galatola, L. A. Lugiato, M. Vadacchino, and N. B. Abraham, Opt. Commun. **69**, 419 (1989).
[5] C. Fabre, E. Giacobino, A. Heidmann, L. A. Lugiato, S. Reynaud, M. Vadacchino, and Wang Kaige, Quantum Opt. **2**, 159 (1990).
[6] L. A. Lugiato and Wang Kaige, Ann. Phys. (Leipzig) **7**, 539 (1990).
[7] L. Wu, H. J. Kimble, J. L. Hall, and H. Wu, Phys. Rev. Lett. **57**, 2520 (1986).
[8] A. Heidmann, R. J. Horowicz, S. Reynaud, E. Giacobino, and C. Fabre, Phys. Rev. Lett. **59**, 2555 (1987).
[9] P. D. Drummond, K. J. McNeil, and D. F. Walls, Opt. Acta **27**, 321 (1980); **28**, 211 (1981).
[10] P. Mandel and T. Erneux, Opt. Acta **29**, 7 (1982).
[11] L. A. Lugiato, C. Oldano, C. Fabre, E. Giacobino, and R. J. Horowicz, Nuovo Cimento D **1**, 959 (1988).
[12] P. Galatola, L. A. Lugiato, M. Vadacchino, and N. B. Abraham, Opt. Commun. **69**, 414 (1989).
[13] P. Mandel, N. P. Pettiaux, Wang Kaige, P. Galatola, and L. A. Lugiato, Phys. Rev. A **43**, 424 (1991).
[14] L. A. Lugiato, P. Galatola, and L. M. Narducci, Opt. Commun. **76**, 276 (1990).
[15] M. J. Collet and D. F. Walls, Phys. Rev. A **32**, 2887 (1985).
[16] P. Galatola, L. A. Lugiato, M. Vadacchino, and N. B. Abraham, in *Proceedings of Dynamics of Nonlinear Optical Systems*, edited by L. Pesquera and F. J. Bermejo (World Scientific, Singapore, 1988), p. 154.
[17] H. P. Yuen and J. H. Shapiro, Opt. Lett. **4**, 334 (1979).
[18] P. Kumar and J. H. Shapiro, Phys. Rev. A **30**, 1568 (1984).
[19] R. E. Slusher, L. M. Hollberg, B. Yurke, J. C. Mertz, and J. F. Valley, Phys. Rev. Lett. **55**, 2409 (1985).
[20] P. Mandel, P. Galatola, L. A. Lugiato, and Wang Kaige, Opt. Commun. **80**, 262 (1991).
[21] M. D. Reid and D. F. Walls, Phys. Rev. A **31**, 1622 (1985).
[22] R. E. Slusher, B. Yurke, P. Grangier, A. La Porta, D. F. Walls, and M. D. Reid, J. Opt. Soc. Am. B **4**, 1453 (1987).
[23] M. D. Reid and D. F. Walls, Phys. Rev. A **31**, 1622 (1985).
[24] D. A. Holm and M. Sargent III, Phys. Rev. A **35**, 2150 (1987).
[25] W. Zhang and D. F. Walls, Phys. Rev. A **41**, 6835 (1990).
[26] M. Brambilla, F. Castelli, L. A. Lugiato, F. Prati, and G. Strini, Opt. Commun. **83**, 367 (1991).
[27] N. B. Abraham, in *Proceedings of Dynamics if Nonlinear Optical Systems* (Ref. [16]), p. 3.
[28] J. M. Gambaudo, P. A. Glendinning, and C. Tresser, J. Phys. (Paris) Lett. **46**, L653 (1985).
[29] P. Glendinning, in *New Directions in Dynamical Systems*, edited by T. Bedford and J. Swift (Cambridge University, Cambridge, England, 1983), pp. 120–149.
[30] E. N. Lorenz, J. Atmos, Sci. **20**, 130 (1963); H. Haken, Phys. Lett. **53A**, 77 (1975)
[31] J. W. Swift and K. Wiesenfeld, Phys. Rev. Lett. **52**, 705 (1984).
[32] Shin-ichi Sato, Masaki Sano, and Yasuij Sawada, Phys. Rev. A **28**, 1654 (1983).
[33] S. Novak and R. G. Frehlich, Phys. Rev. A **26**, 3600 (1982).
[34] Y. Kuramoto and S. Koga, Phys. Lett. **92A**, 1 (1982).

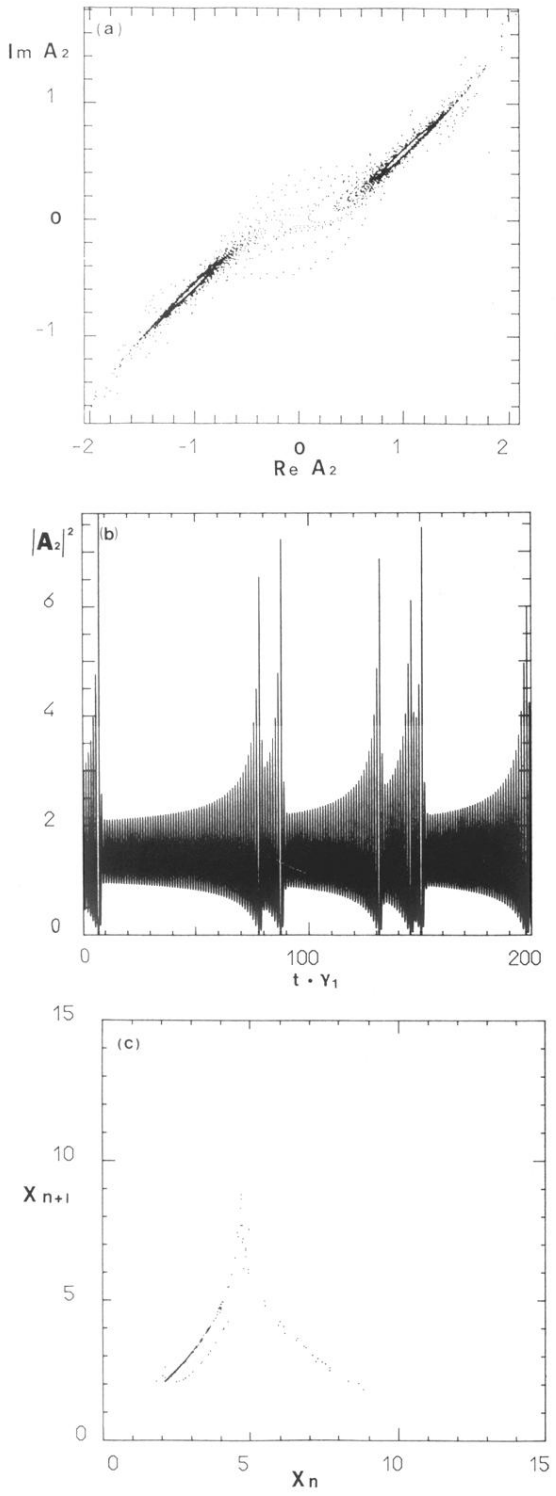

FIG. 5. Lorenz-like chaos for $\mu=1.0$, $\Delta_1=-2.0$, $\Delta_2=5.0$, and $|A_{2s}|^2=1.47$: (a) Orbit in the complex plane of the signal field, (b) intensity evolution in time for the signal field, and (c) Lorenz map for peaks in the intensity of the signal field.